Cone-beam Reconstruction from General Discrete Vertex Sets using Radon Rebinning Algorithms

Frédéric Noo, *Student Member, IEEE*, Rolf Clack, *Member, IEEE*, Michel Defrise
University of Liège (Belgium), University of Utah (U.S.A.), Free University of Brussels (Belgium)

Abstract

This paper addresses image reconstruction in cone-beam tomography from an arbitrary discrete set of positions of the cone vertex. As a first step in the analysis of the problem, we define some measures of how close a discrete vertex set comes to satisfying Tuy's condition [1]. Next, we propose three rebinning algorithms which use Grangeat's formula [2] and Marr's algorithm [3], and are capable of accurate reconstructions. The first algorithm is designed to accurately process cone-beam data finely sampled along a vertex path satisfying Tuy's condition. The second algorithm applies to pair-complete vertex sets. The third algorithm is suited to process any discrete vertex set. The efficacy of the algorithms is illustrated with reconstructions from computer-simulated data using several vertex sets, including a set of randomly placed vertices.

I. Introduction

The cone-beam (CB) reconstruction problem consists of recovering a 3D image from line integrals diverging from vertex points distributed about the object under study. The terminology "vertex point" refers to the position of the x-ray source in area CT or to the focal point of the converging collimator in SPECT imaging. The set of line integrals measured from one vertex point is called a CB projection.

Usually, the vertex points are sampled along a continuous or piecewise continuous trajectory called the "vertex path". Direct CB reconstruction algorithms are based on the discretization of exact or approximate analytical inversion formulae, which are derived assuming that the CB projections are known for all points along the vertex path. The main direct algorithms can be classified as filtered backprojection (FBP) methods or Radon methods.

The most popular FBP method was proposed by Feldkamp et al [4] who derived an algorithm for approximate reconstruction of data sampled along a circular vertex path. Tuy showed [1] that accurate reconstruction is possible if the vertex path is non-tangentially intersected by any plane intersecting the support of the object. Finch [5] established that Tuy's condition is also necessary for accurate reconstructions, thereby demonstrating that a circular vertex path is insufficient in principle. Defrise and Clack [6], and Kudo and Saito [7] derived in 1994 a FBP algorithm, which yields accurate reconstructions from CB projections sampled along any vertex path satisfying Tuy's condition.

Radon methods rely on the estimation of an intermediate function relating the CB data to plane integrals of the object. Different intermediate functions were proposed by Tuy [1], Smith [8] and Grangeat [2]. Tuy's algorithm was implemented by Zeng et al [9] for a path consisting of one circle and two lines orthogonal to the circle. Smith's and Grangeat's approaches were investigated for a circular path [10] and a helical path [11, 12, 13].

The vertex-path model of the CB problem is appealing because Tuy's condition can be used to describe a complete dataset, and there are direct algorithms available for reconstruction from complete data. However, strict adherence to this model can be a limitation in practical situations. First, it can be difficult to satisfy Tuy's condition. For example, in SPECT imaging with a CB collimator, the main concern is to optimize the use of the detector surface without data truncation, and the additional complication of positioning the detector to satisfy Tuy's condition can be prohibitive. Second, the CB measurements might be acquired in such a way that no natural vertex path can be defined. For example, if patient motion were monitored during a CB data acquisition, the vertex points could be viewed as a set of irregularly distributed data points, for which no satisfactory reconstruction algorithm currently exists.

In this paper, we consider CB projections measured for an arbitrary discrete set of vertex points, which may or may not result from the discretization of a vertex path. Existing FBP methods are inherently linked to the notion of a vertex path, and this is also true for Tuy's algorithm. The Radon methods based on Grangeat's or Smith's formula seem amenable to an implementation for general discrete vertex sets. Specifically, the CB data can be used to evaluate the plane integrals of the object for all planes containing the vertices. Assuming that a 3D rebinning method can be devised which uses these values to generate a regular sampling of plane integrals, the 3D object can then be accurately reconstructed by applying the inverse Radon transform.

The problem of CB tomography with discrete data sets has already been investigated by Barrett and Gifford [14]. The algorithm they proposed was based on a decomposition of the 3D image using Fourier functions. The projection-backprojection matrix resulting from

0018-9499/97$10.00 © 1997 IEEE

this decomposition is nearly diagonal, and Barrett and Gifford showed that good estimates of the image can be obtained by simply backprojecting the data, and normalizing the result using the diagonal elements of the projection-backprojection matrix. The approach we adopt in this work is very different. Considering the Radon method based on Grangeat's formula, we firstly derive a rebinning algorithm which yields accurate reconstruction from CB data finely sampled along any vertex path satisfying Tuy's condition. Next, we generalize the approach and propose two rebinning algorithms which are capable of accurate reconstructions from any discrete vertex set. One of these methods was presented at the 1996 IEEE Medical Imaging Conference. The more detailed description here, including the other two rebinning methods, constitute a considerably extended version of the Conference Record paper [15].

The organization of the paper is as follows. In section II, the CB problem with discrete vertex sets is reviewed, and different parameters are defined which measure how close a discrete vertex set comes to satisfying Tuy's condition. The Radon method based on Grangeat's formula is reviewed in section III, and the new rebinning algorithms are presented in section IV. Section V is devoted to simulations. Different computer-simulated data sets are considered to show the ability of the new rebinning algorithms to process arbitrary discrete vertex sets. A brief summary and discussion is given in section VI.

II. Discrete vertex sets

A. CB reconstruction problem

We consider the problem of reconstructing a 3D object represented by a function $f(\underline{x})$ of compact support Ω from CB projections measured for a discrete set of vertex points $\{\underline{a}_1, \underline{a}_2, \ldots, \underline{a}_N\}$. The CB projections

$$g(u, v, \underline{a}_i) = \int_0^\infty dt\, f(\underline{a}_i + t\,\underline{\alpha}) \qquad (1)$$

are collected on a 2D detector located a distance D_i from the vertex point. The coordinates (u, v) on the detector are defined with respect to unit orthogonal axes $\underline{e}_u$ and $\underline{e}_v$, and the point $(u, v) = (0, 0)$ is the projection of $\underline{a}_i$ onto the detector. Each line integral $g(u, v, \underline{a}_i)$ corresponds to a line of direction

$$\underline{\alpha} = (u\,\underline{e}_u + v\,\underline{e}_v - D_i\,\underline{e}_w)/\sqrt{u^2 + v^2 + D_i^2} \qquad (2)$$

connecting the vertex point $\underline{a}_i$ to some point (u, v) on the detector. The unit vector $\underline{e}_w = \underline{e}_u \times \underline{e}_v$ is normal to the detector, and points from the detector towards the vertex point (see figure 1). We assume that the CB projections are not truncated, i.e each line issued from the vertex point and passing through the object meets the detector.

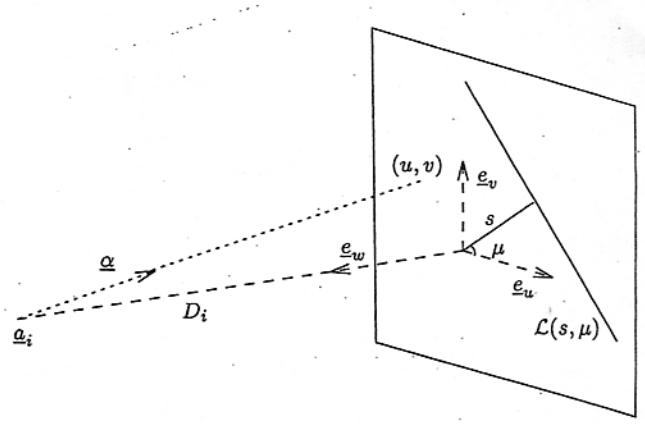

Fig. 1 CB acquisition geometry. The vertex point $\underline{a}_i$ is distance D_i from the detector. Each location (u, v) defines with $\underline{a}_i$ a line of direction $\underline{\alpha}$ along which the density of the object (not shown) is summed, to give the CB projection $g(\underline{a}_i, u, v)$.

B. Closeness to Tuy's condition

No discrete set of vertices can satisfy Tuy's condition because almost all planes crossing the support Ω of $f(\underline{x})$ do not contain any vertex. Different parameters can be defined which give a measure of the degree to which a discrete vertex set $\{\underline{a}_1, \underline{a}_2, \ldots, \underline{a}_N\}$ fails to satisfy Tuy's condition. In this work, we consider two approaches referred to as "vertex pairs approach" and "single vertex approach."

1) Vertex pairs approach

We denote as pair-complete, a discrete vertex set such that for any plane intersecting the support Ω of the object, there are vertices lying on both sides of the plane. With this approach, we consider that accurate reconstruction can only be achieved from pair-complete vertex sets.

Given a pair-complete vertex set, we define ε_p as the smallest distance such that any plane intersecting Ω separates two vertices which are at most a distance ε_p from each other. The parameter ε_p gives some information on the spatial distribution of the vertex points about the object: the smaller the value of ε_p, the better the accuracy that can be expected from the reconstructed image.

The discretization of a vertex path satisfying Tuy's condition leads to a pair-complete vertex set for which ε_p is equal to the largest distance separating two consecutive vertices.

2) Single vertex approach

Another approach to measure the degree to which a discrete vertex set fails to satisfy Tuy's condition consists of calculating the smallest distance ε_s such that any plane intersecting the object is within a distance ε_s of some vertex point. Mathematically, we have

$$\varepsilon_s = \inf\left\{\varepsilon > 0 \,|\, \bigcup_{i=1}^{N} B_\varepsilon(\underline{a}_i) \text{ satisfies Tuy's condition}\right\} \qquad (3)$$

where $B_\varepsilon(\underline{a}_i)$ is the ball of radius ε centered on $\underline{a}_i$.

Vertex points sampled along a path satisfying Tuy's condition admit an ε_s, at most equal to half the maximum distance separating two adjacent points on the path.

Note that there is no single-vertex concept corresponding to pair-complete. Also, the values ε_s and ε_p are not generally related, other than by the inequality $\varepsilon_s \leq \varepsilon_p/2$.

III. Radon method

The Radon method is analogous to the direct Fourier method in parallel-beam tomography, and can be summarized as follows. The CB data are first transformed into the three-dimensional (3D) Radon domain, then in a second step, image reconstruction is performed from the Radon data by applying the 3D Radon inversion formula. In this work, we used Grangeat's formula [2] to transform the CB data so the relevant domain involves the derivative of the Radon transform. For the second step, a slight adaptation of Marr's algorithm [3] was used to complete the reconstruction. See [2, 3, 10, 16] for more detailed descriptions of these concepts.

Each CB projection fills a subset of the Radon domain, and these subsets overlap as more projections are included. The result is a highly non-uniform sampling, with gaps whose size and location depend on the particular vertex set. Since the algorithm of Marr requires a uniform sampling of the Radon domain, a suitable interpolation scheme in the 3D Radon domain is required.

The accuracy of the reconstruction depends on the 3D interpolation scheme and the distance ε_p or ε_s for the vertex set under consideration.

A. Radon transform

Let $\underline{\theta}$ be some unit vector and l some real number. The 3D Radon transform $Rf(\underline{\theta}, l)$ of the image $f(\underline{x})$ is a function which associates to each pair $(\underline{\theta}, l)$ the integral of $f(\underline{x})$ on the plane $\Pi(\theta, l) = \{\underline{x} | \ \underline{x} \cdot \underline{\theta} = l\}$ normal to the direction $\underline{\theta}$ and a distance l from the origin.

$$Rf(\underline{\theta}, l) = \iint_{\underline{x} \in \Pi(\underline{\theta}, l)} d\Pi \, f(\underline{x}) \tag{4}$$

The inversion of the 3D Radon transform can be performed in a stable way provided a complete sampling of the Radon domain is available. The image $f(\underline{x})$ can be reconstructed at any point $\underline{x} \in \Omega$ provided its plane integrals are known for all planes intersecting Ω.

B. Grangeat's formula

Grangeat's formula relates the CB projection data $g(u, v, \underline{a}_i)$ to the derivative of the Radon transform

$$R'f(\underline{\theta}, l) = \frac{\partial}{\partial l} Rf(\underline{\theta}, l) \tag{5}$$

For a fixed CB projection, consider a straight line $\mathcal{L}(s, \mu)$ (see figure 1) on the detector which makes an angle μ with the v-axis and lies a distance s from the origin $(u, v) = (0, 0)$. Define $g_s(u, v, \underline{a}_i)$ as the scaled CB projection

$$g_s(u, v, \underline{a}_i) = \frac{D_i}{\sqrt{u^2 + v^2 + D_i^2}} g(u, v, \underline{a}_i) \tag{6}$$

and let $r(s, \mu)$ represent the sum of $g_s(u, v, \underline{a}_i)$ along $\mathcal{L}(s, \mu)$, so

$$r(s, \mu) = \int_{(u,v) \in \mathcal{L}(s,\mu)} d\mathcal{L} \ g_s(u, v, \underline{a}_i) \tag{7}$$

Grangeat showed that $r(s, \mu)$ is related to the derivative of $Rf(\underline{\theta}, l)$ where the plane $\Pi(\underline{\theta}, l)$ is defined by the vertex point $\underline{a}_i$ and the line $\mathcal{L}(s, \mu)$. Specifically,

$$R'f(\underline{\theta}, l) = \frac{s^2 + D_i^2}{D_i^2} \frac{\partial}{\partial s} r(s, \mu) \tag{8}$$

where

$$\underline{\theta} = (D_i \cos\mu \, \underline{e}_u + D_i \sin\mu \, \underline{e}_v + s \, \underline{e}_w)/\sqrt{s^2 + D_i^2} \tag{9}$$

and

$$l = \underline{\theta} \cdot \underline{a}_i \tag{10}$$

Thus each projection is processed as follows: (i) pointwise multiplication by $D_i/\sqrt{u^2 + v^2 + D_i^2}$ to obtain $g_s(u, v, \underline{a}_i)$, (ii) forward projection in the detector plane to form the sinogram $r(s, \mu)$, (iii) differentiation of the sinogram rows (the s-direction) followed by a scaling by $(s^2 + D_i^2)/D_i^2$. The result yields Radon samples $R'f(\underline{\theta}, l)$ for planes $\Pi(\underline{\theta}, l)$ defined geometrically by the lines $\mathcal{L}(s, \mu)$ and given explicitly by the formula for $\underline{\theta}$ and l above.

C. Marr's algorithm

Marr's algorithm provides an efficient FBP method for inverting the Radon transform $Rf(\underline{\theta}, l)$, or the first derivative of the Radon transform. The vector $\underline{\theta}$ is parameterized using spherical coordinates

$$\underline{\theta} = (\cos\phi \, \sin\theta, \sin\phi \, \sin\theta, \cos\theta) \tag{11}$$

and the image $f(\underline{x})$ is recovered by performing successive 2D backprojections over the variables θ and ϕ. Writing $\underline{x} = (x_1, x_2, x_3)$, we have

$$f(\underline{x}) = \frac{1}{2\pi} \int_0^\pi d\phi \ p(\phi, t, x_3)|_{t = x_1 \cos\phi + x_2 \sin\phi} \tag{12}$$

$$p(\phi, t, x_3) = -\frac{1}{2\pi} \int_0^\pi d\theta \ \sin\theta \frac{\partial}{\partial l} R'f(\underline{\theta}, l)\Big|_{l = t \sin\theta + x_3 \cos\theta} \tag{13}$$

Observe that the derivative data $R'f(\underline{\theta}, l)$ needs to be differentiated once, then backprojected onto a series of vertical planes, one for each ϕ, with vertical x_3-axis and transverse t-axis. The resulting function $p(\phi, t, x_3)$ is then regarded as a set of sinograms in t and ϕ, and backprojected in horizontal planes (one for each x_3) to obtain $f(\underline{x})$.

IV. Rebinning algorithms

The Radon data $R'f(\underline{\theta}, l)$ obtained from the CB projections must be rebinned into an array, called the *Radon array*, of equally spaced samples $\Delta\theta$, $\Delta\phi$, and Δl in preparation for Marr's algorithm. The value at a particular triple (θ, ϕ, l) in the array is found by interpolating from values on nearby planes obtained from the CB projection data. The rebinning schemes described below differ from the methods of [10, 11, 12, 13] which have all been developed for vertex sets corresponding to specific vertex path.

A. Vertex-path algorithm

The interpolation scheme presented in this section is designed to process CB projections finely sampled along an arbitrary vertex path satisfying Tuy's condition. The vertex path consists of $M \ll N$ continuous path segments, along which the N vertices $\underline{a}_i$ are considered as ordered samples along the path. Except possibly for those $2M$ values of i which correspond to segment endpoints, the vertex points $\underline{a}_i$ and $\underline{a}_{i+1}$ form a pair of close vertices.

The values of the Radon array are calculated by successively processing the CB projections along the vertex path. Each pair of close vertices $\underline{a}_i$ and $\underline{a}_{i+1}$ is used for estimating $R'f$ for all planes which intersect the line segment $[\underline{a}_i, \underline{a}_{i+1}]$ connecting $\underline{a}_i$ to $\underline{a}_{i+1}$. Let $\Pi(\underline{\theta}, l)$ be such a plane. Using the method of section IV.D, we firstly select two nearby planes $\tilde{\Pi}_i$ and $\tilde{\Pi}_{i+1}$ which respectively contain the vertices $\underline{a}_i$ and $\underline{a}_{i+1}$. Next, we apply Grangeat's formula to the CB projections $g(\underline{a}_i, u, v)$ and $g(\underline{a}_{i+1}, u, v)$, to calculate $R'f(\tilde{\Pi}_i)$ and $R'f(\tilde{\Pi}_{i+1})$. Since the vertices are close together and also close to $\Pi(\underline{\theta}, l)$, the Radon sample $R'f(\underline{\theta}, l)$ can be accurately estimated as a linear combination of $R'f(\tilde{\Pi}_i)$ and $R'f(\tilde{\Pi}_{i+1})$:

$$R'f(\underline{\theta}, l) = R'f(\tilde{\Pi}_i) + w(\underline{\theta}, l, \underline{a}_i, \underline{a}_{i+1}) \left(R'f(\tilde{\Pi}_{i+1}) - R'f(\tilde{\Pi}_i) \right) \quad (14)$$

where

$$w(\underline{\theta}, l, \underline{a}_i, \underline{a}_{i+1}) = \frac{l - \underline{a}_i \cdot \underline{\theta}}{(\underline{a}_{i+1} - \underline{a}_i) \cdot \underline{\theta}} \quad (15)$$

Note that $(\underline{a}_{i+1} - \underline{a}_i) \cdot \underline{\theta} \neq 0$ because $\Pi(\underline{\theta}, l)$ intersects $[\underline{a}_i, \underline{a}_{i+1}]$.

We observe that each plane integral is estimated at least once because the vertex path satisfies Tuy's condition. Usually, the Radon values $R'f(\underline{\theta}, l)$ are calculated several times, corresponding to multiple intersections of $\Pi(\underline{\theta}, l)$ with the path. Different estimates of the same plane integral are summed during the rebinning process. A weighting array is generated which counts the number of estimates for each plane, and the Radon array is normalized after processing the last pair of close vertices.

B. Vertex-pairs algorithm

The vertex-pairs algorithm is designed to process CB data associated with any pair-complete discrete vertex set. The principle of the rebinning scheme is the same as the one used in the vertex path algorithm, namely plane integrals are estimated using pairs of close vertices. Since the vertex set is no longer considered as a set of ordered points, the main problem consists of defining which pairs of vertices should be processed to ensure all values of $R'f$ in the Radon array are estimated with good accuracy.

The pair-completeness of the vertex set ensures that there exists some distance ε_p such that any plane through the object is separated by two vertices at most a distance ε_p from each other. Therefore, the Radon array can be generated using all pairs of vertices within a distance ε_p from each other.

In practice, the distance ε_p may be inappropriate for estimating planes which are normal to some particular direction $\underline{\theta}$. Some directional property of the vertex set needs to be included during the rebinning process. We begin by calculating for each direction $\underline{\theta}$ the smallest distance $\varepsilon_p(\underline{\theta})$ such that any plane through the object with normal $\underline{\theta}$ is separated by two vertices at most a distance $\varepsilon_p(\underline{\theta})$ from each other. Clearly, $\varepsilon_p(\underline{\theta}) \leq \varepsilon_p$. Next, we begin the rebinning process. We isolate each pairs of vertex points within a distance ε_p from each other. Given a fixed pair of such vertices $\underline{a}_i$ and $\underline{a}_j$, $i \neq j$, we select the directions $\underline{\theta}$ for which the distance between $\underline{a}_i$ and $\underline{a}_j$ is smaller than $\varepsilon_p(\underline{\theta})$, and we estimate $R'f$ for all planes normal to any of these directions, and separating $\underline{a}_i$ and $\underline{a}_j$.

The estimation of $R'f$ for a specific plane $\Pi(\underline{\theta}, l)$ is carried out in the same way as for the vertex path algorithm. Two nearby planes $\tilde{\Pi}_i$ and $\tilde{\Pi}_j$ are identified which separately contain $\underline{a}_i$ and $\underline{a}_j$ (see section IV.D); Grangeat's formula is applied to the CB projections $g(\underline{a}_i, u, v)$ and $g(\underline{a}_j, u, v)$ to calculate $R'f(\tilde{\Pi}_i)$ and $R'f(\tilde{\Pi}_j)$; and $R'f(\underline{\theta}, l)$ is obtained by linear interpolation.

Again plane integrals can be estimated several times so the multiple estimates are summed and normalized by a counting array after the last pair of close vertices has been processed.

C. Single-vertex algorithm

The single-vertex algorithm is suited to process any discrete vertex set. The basic idea is to consider each direction $\underline{\theta}$ separately, and obtain values $R'f(\underline{\theta}, l)$ in the Radon array from CB projection data whose vertex points lie within a distance $\Delta(\underline{\theta})$ from the plane $\Pi(\underline{\theta}, l)$. The interpolating distance $\Delta(\underline{\theta})$ is defined in terms of the particular vertex set.

We begin by defining $\varepsilon_s(\underline{\theta})$ as the largest distance between some plane through the object with normal $\underline{\theta}$, and the nearest vertex point to it. Mathematically,

$$\varepsilon_s(\underline{\theta}) = \sup_{l \in L_{\underline{\theta}}} \left\{ \min_{i=1,\cdots,N} |l - \underline{a}_i \cdot \underline{\theta}| \right\} \quad (16)$$

where

$$L_{\underline{\theta}} = \{l \,|\, l = \underline{\theta} \cdot \underline{x},\ x \in \Omega\} \tag{17}$$

Clearly the definition of $\varepsilon_s(\underline{\theta})$ generalizes the definition of ε_s given in section II.B.2, with $\varepsilon_s = \sup\{\varepsilon_s(\underline{\theta})\}$. The interpolating distance $\Delta(\underline{\theta})$ is defined as $\Delta(\underline{\theta}) = k\,\varepsilon_s(\underline{\theta})$ where $k \geq 1$ is a tuning parameter to be discussed below.

The 3D interpolation scheme proceeds as follows. First, for each direction $\underline{\theta}$ in the Radon array, the value $\varepsilon_s(\underline{\theta})$ is calculated by sorting the relative distances $\underline{a}_i \cdot \underline{\theta}$ of each vertex point $\underline{a}_i$ projected onto the line segment $L_{\underline{\theta}}$, and finding the maximum distance between successive points on this line. Care must be taken at the endpoints of $L_{\underline{\theta}}$, especially if no points project outside this segment. Then, with $\Delta(\underline{\theta})$ defined, each vertex point $\underline{a}_i$ is successively processed with five operations:

- the set of planes $\Pi(\underline{\theta}, l)$ of the Radon array are selected which lie within a distance $\Delta(\underline{\theta})$ of $\underline{a}_i$,
- for each selected plane $\Pi(\underline{\theta}, l)$, a nearby plane $\tilde{\Pi}(\tilde{\underline{\theta}},\ \underline{a}_i \cdot \tilde{\underline{\theta}})$ containing the vertex point $\underline{a}_i$ is identified using the method described in section IV.D below,
- the value $R'f$ for $\Pi(\underline{\theta}, l)$ is estimated from $R'f$ for $\tilde{\Pi}$ using Grangeat's formula and the CB projection $g(\underline{a}_i, u, v)$,
- the estimated value of $R'f(\underline{\theta}, l)$ is multiplied by a weight $w(\underline{\theta}, l, \underline{a}_i)$ depending on the distance $d = |l - \underline{a}_i \cdot \underline{\theta}|$ between the plane $\Pi(\underline{\theta}, l)$ and the vertex point $\underline{a}_i$:

$$w(\underline{\theta}, l, \underline{a}_i) = (\Delta(\underline{\theta}) - d)/\Delta(\underline{\theta}) \tag{18}$$

- the weight $w(\underline{\theta}, l, \underline{a}_i)$ is added to location $(\underline{\theta}, l)$ of a weighting Radon array, so that the estimated values of $R'f$ can be normalized after the last vertex point has been processed.

The tuning parameter k must be chosen so as to ensure a good compromise between the average number of vertex points contributing to each Radon plane, and the accuracy of the estimate of $R'f$ obtained from these relatively distant planes. This trade-off is strongly influenced by the signal to noise ratio in the CB data. For the results shown in section V below, the value $k = 2$ was chosen.

D. Interpolation from a single projection

The three rebinning methods described above rely at some point on the estimation of $R'f$ for a given plane $\Pi(\underline{\theta}, l)$ from the CB projection measured for a vertex point $\underline{a}_i$. We describe in this section the method which has been used to achieve this estimation.

Using Grangeat's formula, $R'f$ can be calculated for all planes containing the vertex $\underline{a}_i$. Since in general $\underline{a}_i \notin \Pi$, the problem reduces to approximating $\Pi(\underline{\theta}, l)$ by some plane $\tilde{\Pi}(\tilde{\underline{\theta}},\ \underline{a}_i \cdot \tilde{\underline{\theta}})$ containing $\underline{a}_i$.

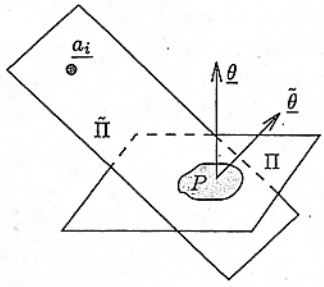

Fig. 2 Approximating Π with $\tilde{\Pi}$. Consider a plane Π and a vertex point $\underline{a}_i \notin \Pi$. A good estimate for $R'f$ on Π is given by the value of $R'f$ on the plane $\tilde{\Pi}$ which contains the vertex point $\underline{a}_i$, some central point P of interest on Π, and is oriented so as to have a minimum angle with Π.

To achieve this goal we rely on knowledge of the image support. We localize some region of interest in the plane $\Pi(\underline{\theta}, l)$ and select a central point P in this region. Then, the plane $\tilde{\Pi}$ is chosen to contain the vertex point $\underline{a}_i$, the central point P, and oriented such that its angle with the plane Π is minimized (see figure 2). Mathematically, the unit vector $\tilde{\underline{\theta}}$ normal to $\tilde{\Pi}$ is given by the relation

$$\tilde{\underline{\theta}} = \frac{\underline{\theta} - (\underline{\theta} \cdot \underline{p})\underline{p}}{||\underline{\theta} - (\underline{\theta} \cdot \underline{p})\underline{p}||} \tag{19}$$

where the unit vector $\underline{p}$ is along the line connecting the point P to the vertex point. If $\underline{p}$ and $\underline{\theta}$ are colinear then $\tilde{\Pi}$ must necessarily be perpendicular to Π. In this case, equation (19) cannot be used, but any $\tilde{\underline{\theta}}$ perpendicular to $\underline{\theta}$ may be chosen. In practice this situation occurs rarely because $\underline{a}_i$ is typically close to Π and far from P.

E. Efficient use of Grangeat's formula

The three rebinning algorithms proposed in sections IV.A, IV.B and IV.C make efficient use of Grangeat's formula in the sense that the sinogram for each CB projection, equation (7), is precomputed before being involved in the rebinning process. Specific line integrals required during 3D interpolation are computed by bilinear interpolation in the sinograms of the detectors.

The computation of a particular sinogram is computationally intensive. To be efficient, the rebinning algorithms must be implemented in such a way that the sinogram of each CB projection is only calculated once.

For the vertex-path algorithm, the vertex points are processed by pairs of ordered vertices $\underline{a}_i$ and $\underline{a}_{i+1}$. The sinogram for the CB projection $g(\underline{a}_{i+1}, u, v)$ is computed at the time the pair $(\underline{a}_i, \underline{a}_{i+1})$ is involved, and is stored until after the next pair has been processed. The sinogram for $g(\underline{a}_i, u, v)$ is known from the processing of the previous pair, unless $\underline{a}_i$ begins a new continuous path segment in which case the sinogram of $g(\underline{a}_i, u, v)$ has not yet been computed.

For the vertex-pair algorithm, the vertex points are processed by pairs of non-ordered points. The approach that was adopted was to precompute and store the sinograms for all CB projections before rebinning the data.

For the single-vertex algorithm, the vertex points are also considered as non-ordered, but each CB projection is processed independently of the other projections, and a particular sinogram needs only be computed at the time the corresponding vertex point is involved in the rebinning scheme.

V. Simulations

The aim of the simulation studies is to illustrate the comparative performance of the three new rebinning algorithms, and to demonstrate the possibility to accurately reconstruct CB data acquired with arbitrary discrete sets of vertex points.

A. Discretization

The phantom used was the standard 3D Shepp phantom [17]. Four discrete vertex sets were considered, and all consisted of vertex points located on the surface of an imaginary cylinder of radius 350mm. The simulated detector was always parallel to the symmetry axis of the cylinder, and a distance $D = 700$mm from the vertex point. The projection data were generated on a grid of 128×128 square pixels each of area 4mm^2. The reconstructed images contained $100 \times 100 \times 100$ cubic voxels of volume 8mm^3 each.

The intermediate sinograms were computed using linogram techniques. Each linogram contained 256 angular samples and 256 radial samples, with a radial sampling distance ranging from $\Delta s = 4.0$ mm to $\Delta s = 2.83$ mm.

The Radon array contained 120×120 directions $\underline{\theta}$ corresponding to a uniform sampling of the polar and azimuthal angles (θ, ϕ) over a range $[0, \pi] \times [0, \pi]$. For each direction $\underline{\theta}$ there were 128 radial samples, at a radial sampling distance of $\Delta l = 1.5$mm.

The derivative filters were always applied in object space using the convolution kernel $(0, \ldots, 0, 1/2, 0, -1/2, 0, \ldots, 0)$ which corresponds to the centered scheme:

$$\frac{df}{dx}(i\Delta x) = \frac{f((i+1)\Delta x) - f((i-1)\Delta x)}{2\Delta x} \qquad (20)$$

B. Helix path

The first vertex set consisted of 256 vertex points finely sampled along a 2-turn helix of pitch 130mm. Figures 3a and 3b respectively show the standard vertical slices through the reconstructed phantom obtained using the vertex-path algorithm and the single-vertex algorithm. The vertex-pairs approach was not considered because of its similarity to the vertex-path approach for this data set. The parameter $\varepsilon_p(\underline{\theta})$ was independent of $\underline{\theta}$ and equal to 17.28mm, the sampling distance along the path.

The vertex-path and single-vertex reconstructions are of similar quality. This is because $\varepsilon_s = 7.83$mm is close to half the sampling distance along the path, and because the single-vertex algorithm is executed with a linear interpolating function of width $\Delta(\underline{\theta}) = 2\varepsilon_s(\underline{\theta})$. The vertex-path and single-vertex algorithms both interpolate in some sense between pairs of adjacent points along the path. The histogram of $\varepsilon_s(\underline{\theta})$ for the helix data set is given in figure 3c.

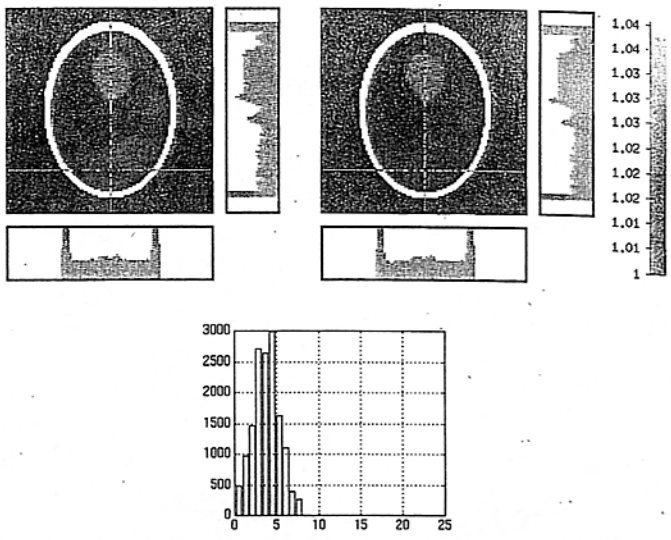

Fig. 3 Reconstruction of the helix data: (a, top left) vertex-path algorithm (b, top right) single-vertex algorithm (c, bottom) histogram of $\varepsilon_s(\underline{\theta})$. For this application, both algorithms interpolate in some sense between pairs of close vertices and the results are similar.

C. Five-circles path

The second vertex set consisted of 225 CB projections sampled along five parallel circles a distance 49mm from each other. The number of vertices on each circle was 45 so that the distance between two adjacent points on a circle was about the same as the distance between the circles.

The five-circle vertex path does not satisfy Tuy's condition, and a complete Radon array cannot be built using the vertex-path algorithm. Most algorithms available in the literature would fail to provide satisfactory reconstructions from such a data set, unless extrapolation methods in the Radon array were applied [10]. The vertex-pairs and single-vertex algorithms gave good reconstructions from the five-circles data set. The results are shown respectively in figures 4a and 4b. The vertex-pairs reconstruction seems slightly better than the single-vertex reconstruction. The parameter $\varepsilon_p(\underline{\theta})$ was close to 49mm for all directions. All vertices are paired, and the interpolation between close vertices using the vertex-pairs approach provides a very accurate result.

The histogram of $\varepsilon_s(\underline{\theta})$ (figure 4c) for the 5-circles data set can be compared with the histogram for the helix data set (figure 3c).

D. Random vertex set

The third vertex set consisted of 256 points placed randomly on the wall of the imaginary cylinder of radius 350mm. The points were distributed uniformly over a

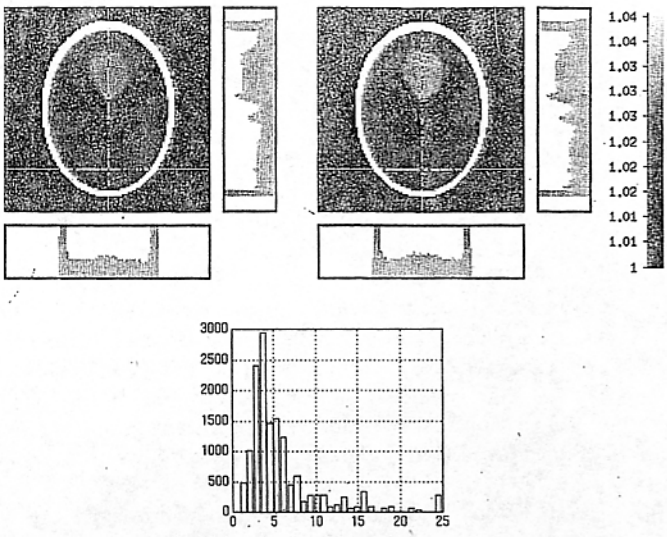

Fig. 4 Reconstruction of the 5-circles data: (a, top left) vertex-pairs algorithm (b, top right) single-vertex algorithm (c, bottom) histogram of $\varepsilon_s(\underline{\theta})$. All vertices are paired and the vertex-pairs algorithm provides a very accurate result.

height of 220mm and uniformly in angle, and are plotted in figure 5.

Clearly, no natural path can be defined which contains all vertices. No existing algorithm in the literature could accurately process such a data set, however the vertex-pairs and single-vertex algorithms can process any set of unordered data points. The results are respectively shown in figures 6a and 6b.

The vertex-pair reconstruction is slightly worse than the single-vertex reconstruction. The single-vertex approach has the benefit of using isolated (unpaired) vertices that may be near Radon planes, whereas the vertex-pairs approach must find two vertices surrounding the Radon plane. The histogram of $\varepsilon_p(\underline{\theta})$ and $\varepsilon_s(\underline{\theta})$ are shown in figure 6c and 6d.

The histogram of $\varepsilon_s(\underline{\theta})$ can be compared with the histograms of figures 3c and 4c. The average values of $\varepsilon_s(\underline{\theta})$ for the random set and five-circles set are slightly larger than for the helix vertex set, which seems to correlate with the observation that the resolution of images 6b and 4b are slightly poorer than the resolution of image 3b.

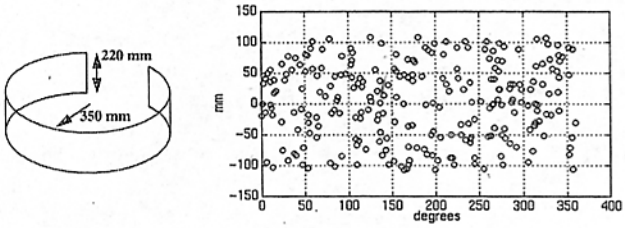

Fig. 5 Example of a discrete set of unordered vertex points. The vertices are randomly distributed on the wall of an imaginary cylinder.

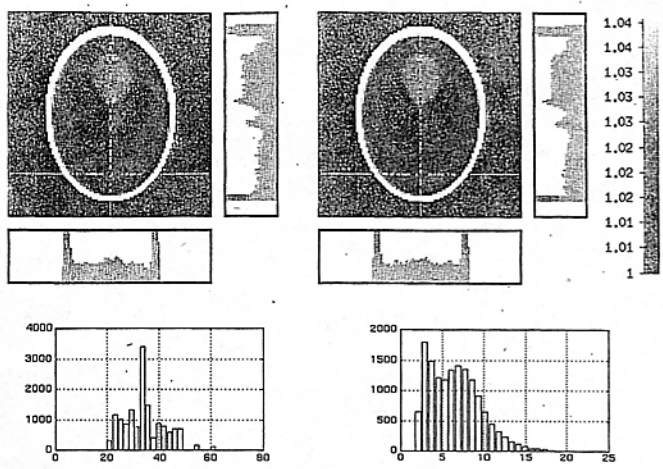

Fig. 6 Reconstruction from the random vertex data: (a, top left) vertex-pairs algorithm (b, top right) single-vertex algorithm (c, bottom left) histogram of $\varepsilon_p(\underline{\theta})$ (d, bottom right) histogram of $\varepsilon_s(\underline{\theta})$. The single-vertex algorithm has the benefit of using isolated (unpaired) vertices that may be near Radon planes, which results in a better reconstruction.

E. Circle path

For the last experiment, the vertex set was 256 points uniformly sampled along a circle about the object. The circle path does not satisfy Tuy's condition and only approximate reconstruction is possible. The FDK algorithm of Feldkamp et al [4] yields the result of figure 7a. The discrete vertex set is not pair-complete so only the single-vertex algorithm was considered. (The Radon method can still be applied in general if some extrapolation method is used to fill in the holes in an incomplete Radon array. We do not consider extrapolation methods in this paper.) The single-vertex reconstruction is shown in figure 7b. The result is more accurate than the FDK result, which displays the well-known reduced intensity away from the center in the vertical direction. The single-vertex algorithm gives estimates for any plane integral through the object and results in a good reconstruction when considering the 3D Shepp phantom whose axial frequency content is low.

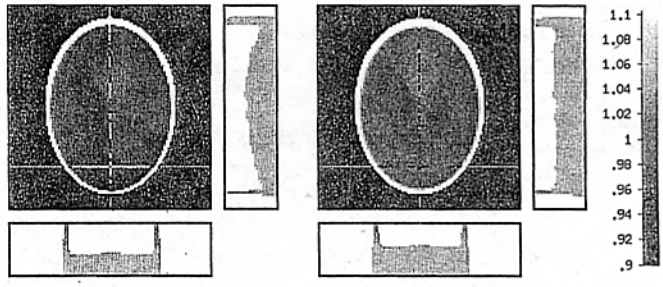

Fig. 7 Reconstruction of the circle data: (a, left) FDK algorithm (b, right) single-vertex algorithm. The single-vertex algorithm gives estimates for any plane integral through the object and results in a good reconstruction of the 3D Shepp phantom. Note that a less compressed greyscale is used, to avoid exaggerating the FDK artifacts in the vertical profile.

VI. Discussion and conclusion

Three new rebinning algorithms have been proposed and were implemented using the Radon derivative domain using Grangeat's formula, and Marr's algorithm to perform the Radon inversion. Simulation studies verified that these methods gave good recontructions of the 3D Shepp phantom. The vertex-path algorithm was shown to effectively process finely sampled data along a vertex path. This method was generalized to the vertex-pairs algorithm, which was shown to be capable of accurate reconstruction for any pair-complete data set. The single-vertex algorithm is the most general algorithm since it applies to any arbitrary vertex set to yield near-optimal reconstruction.

The essential aspect of these algorithms is the interpolation procedures used to obtain estimates in the Radon domain. The vertex-pair algorithm has the advantage of always interpolating between two planes surrounding the plane of interest, whereas the single-vertex approach allows unpaired vertices which are close to the plane of interest to provide estimates.

Other components of the implementations described here are not as crucial to the reconstruction quality. However some minor improvements in reconstruction time might be achieved by replacing the Marr algorithm with a 3D linogram approach [17], or by using Fourier reconstruction with gridding [18]. We have also implemented the vertex-path method using Smith's approach [8] and the corresponding Radon domain. The reconstructions were of comparable quality to those reported here.

A close examination of the interpolation methods described in this work suggests that the ε_p or ε_s definitions are too naive to yield a quantitative predictor of reconstructed resolution possible with specific discrete vertex sets. Figure 2 illustrates that the approximation made by the choice of $\tilde{\Pi}$ is far better than what is suggested by the distance from the vertex point $\underline{a}_i$ to the plane Π. The distance from P to $\underline{a}_i$ and the size of the field of view both need to be taken into account also. However, for the single-vertex algorithm, we observe that the directional vertex sampling $\varepsilon_s(\underline{\theta})$ is a good tool for the comparison of discrete vertex sets.

VII. Acknowledgement

F. Noo is a Research Assistant and M. Defrise is a Research Director, both supported by the Belgian National Fund for Scientific Research. R. Clack and F. Noo were partially supported by a grant from the Whitaker Foundation, U.S.A.

VIII. References

[1] H. Tuy, "An inversion formula for cone-beam reconstruction", SIAM J. Appl. Math., 43, 546-522, 1983.

[2] P. Grangeat, "Mathematical framework of cone-beam 3D reconstruction via the first derivative of the Radon transform", Mathematical methods in tomography, Herman, Louis and Natterer (eds.), Lecture Notes in Mathematics 1497, 66-97, Springer-Verlag, Berlin 1991.

[3] Marr R, Chen C, Lauterbur P, "On two approaches to 3D reconstruction in NMR zeugmatography", Proc. Math. Aspect of CT, Oberwolfach (FRG), 1980, Herman G, Natterer F (eds), 225-240, Springer-Verlag 1981.

[4] L. A. Feldkamp, L. C. Davis, J. W. Kress, "Practical cone-beam algorithm", J. Opt. Soc. Amer. A, A6, 612-619, 1984.

[5] D. Finch, "Cone-beam reconstruction with sources on a curve", SIAM J. Appl. Math., 45, 665-673, 1985.

[6] M. Defrise and R. Clack, "A cone-beam reconstruction algorithm using shift variant filtering and cone-beam backprojection", IEEE Trans. Med. Imag., 13, 186-195, 1994.

[7] H. Kudo, T. Saito, "Derivation and implementation of a cone-beam reconstruction algorithm for nonplanar orbits", IEEE Trans. Med. Imag., 13, 196-211, 1994.

[8] B. D. Smith, "Image reconstruction from cone-beam projections: Necessary and sufficient conditions and reconstruction methods", IEEE Trans. Med. Imag., 4, 14-28, 1985.

[9] G. L. Zeng, R. Clack, G. T. Gullberg, "Implementation of Tuy's cone-beam inversion formula", Phys. Med. Biol., 39(3), 493-507, 1994.

[10] P. Grangeat, *Analyse d'un système d'imagerie 3D par reconstruction à partir de radiographies X en géometrie conique*, Ph.D. Thesis, Ecole Nationale Supérieure des Télécommunications, France, 1987.

[11] H. Kudo, T. Saito, "Feasible cone-beam scanning methods for exact reconstruction in three-dimensional tomography", J. Opt. Soc. Am. A, 7, 2169-2183, 1990.

[12] Y. Weng, G. L. Zeng, G. T. Gullberg, "A reconstruction algorithm for helical cone-beam SPECT", IEEE Trans. Nucl. Sci, 40, 1092-1101, 1993.

[13] J. Eriksson, P. Danielson, "Helical scan 3D reconstruction using the linogram method", Proc. of International Meeting on Fully 3D Image Reconstruction in Radiology and Nuclear Medicine, Aix-les-Bains, France, 287-290, 1995.

[14] H. H. Barrett, H. Gifford, "Cone-beam tomography with discrete data sets", Phys. Med. Biol., 39(3), 451-476, 1994.

[15] F. Noo, R. Clack, M. Defrise, "Cone-beam reconstruction from general discrete vertex sets", IEEE Conf. Record of the 1996 Nuclear Science Symposium and Medical Imaging Conference, Anaheim, CA, (to appear), 1996.

[16] C. Axelsson, P. E. Danielsson, "3D reconstruction from cone-beam data in $O(N^3 \log N)$ time", Phys. Med. Biol., 39, 477-491, 1994.

[17] C. Axelsson-Jacobson, *Fourier methods in 3D-reconstruction from cone-beam data*, Ph.D. Thesis, Dept of Elect. Eng., Linköping University, S-581 83 Linköping, Sweden, 1996.

[18] S. Schaller, T. Flohr, "An efficient Fourier method for 3D Radon inversion in exact cone-beam CT reconstruction", IEEE Conf. Record of the 1996 Nuclear Science Symposium and Medical Imaging Conference, Anaheim, CA, (to appear), 1996.